Princeton Plasma Physics Laboratory

PPPL- 4605

PPPL- 4605

Modification of Particle Distributions by MHD Instabilities II

Roscoe B. White

March, 2011

Prepared for the U.S. Department of Energy under Contract DE-AC02-09CH11466.

Princeton Plasma Physics Laboratory
Report Disclaimers

Full Legal Disclaimer

Trademark Disclaimer

PPPL Report Availability

Princeton Plasma Physics Laboratory:

http://www.pppl.gov/techreports.cfm

Office of Scientific and Technical Information (OSTI):

http://www.osti.gov/bridge

Related Links:

U.S. Department of Energy

Office of Scientific and Technical Information

Fusion Links

Modification of particle distributions by MHD instabilities II

R. B. White[1]

[1]*Plasma Physics Laboratory, Princeton University,*

P.O.Box 451, Princeton, New Jersey 08543

(Dated: February 25, 2011)

Abstract

The modification of particle distributions by low amplitude magnetohydrodynamic modes is an important topic for magnetically confined plasmas. Low amplitude modes are known to be capable of producing significant modification of injected neutral beam profiles, and the same can be expected in burning plasmas for the alpha particle distributions. Flattening of a distribution in an island due to phase mixing and portions of phase space becoming stochastic lead to modification of the particle distribution, a process extremely rapid in the time scale of an experiment but still very long compared to the time scale of guiding center simulations. Large amplitude modes can cause profile avalanche and particle loss. Thus it is very valuable to be able to predict the temporal evolution of a particle distribution produced by a given spectrum of magnetohydrodynamic modes. In this paper we further develop and investigate the use of a new method of determining domains of phase space in which good KAM surfaces do not exist and use this method to examine a well documented case of profile modification by instabilities.

PACS numbers: 52.25.Fi, 52.25.Gj

I. INTRODUCTION

The resonant interaction of magnetohydrodynamic (MHD) modes and particle distributions can produce significant modification of the distribution and even induce large scale particle loss through profile avalanche, and is an important topic for magnetically confined plasmas. Low amplitude modes are known to be capable of producing significant modification of injected neutral beam profiles [1–3], and the same can be expected in burning plasmas for the alpha particle distributions. Since magnetic field ripple is a strong function of position, increasing rapidly near the plasma edge, this can lead to an increase of estimates for stochastic trapped particle ripple loss. Portions of phase space becoming stochastic lead to modification of the particle distribution, a process extremely rapid on the time scale of an experiment but still very long compared to the time scale of guiding center simulations, typically hundreds of hours of computing time to find saturated profiles under the action of a particular mode spectrum. Thus it is very valuable to be able to predict the evolution of a particle distribution produced by a given spectrum of MHD modes, and to ascertain which modes are relevant for profile modification. In a previous paper[4] we introduced a method for determining the evolution of the particle distribution without carrying out a full guiding center simulation, by introducing a new technique for exactly determining the location of resonances and the widths of the islands produced. This paper consists of a study of a particular well diagnosed discharge in DIII-D[2, 3]. In section II we review the method of resonance determination. In section III we discuss the equilibrium, modes and particle distribution in DIII-D shot 122117, and in section IV we show the resonances produced by the observed mode spectrum. Section V concerns the time evolution of orbit pairs used to find domains of non KAM surfaces, and in section VI we calculate the modified particle distribution and losses caused by the modes. Section VII is the conclusion.

II. RESONANCE DETERMINATION

Using the guiding center drift approximation a particle orbit in an axisymmetric system is completely described by the values of the toroidal canonical momentum P_ζ, the energy E and the magnetic moment μ. Particle spatial coordinates are given by ψ_p, θ, ζ, respectively the poloidal flux coordinate, and the poloidal and toroidal angles. The magnetic field is

given by

$$\vec{B} = g\nabla\zeta + I\nabla\theta + \delta\nabla\psi_p, \tag{1}$$

and in an axisymmetric equilibrium using straight field line Boozer coordinates g and I are functions of ψ_p only. The trajectory of the particle motion in the poloidal plane and the toroidal precession of the orbit are independent of the function δ.

The guiding center Hamiltonian is

$$H = \rho_\parallel^2 B^2/2 + \mu B + \Phi, \tag{2}$$

where $\rho_\parallel = v_\parallel/B$ is the normalized parallel velocity, μ is the magnetic moment, and Φ the electric potential. The field magnitude B and the potential may be functions of ψ_p, θ and also ζ if axisymmetry is broken. Canonical momenta are

$$P_\zeta = g\rho_\parallel - \psi_p, \qquad P_\theta = \psi + \rho_\parallel I, \tag{3}$$

where ψ is the toroidal flux, with $d\psi/d\psi_p = q(\psi_p)$, the field line helicity.

The equations of motion in Hamiltonian form are

$$\begin{aligned} \dot{\theta} &= \frac{\partial H}{\partial P_\theta} \qquad & \dot{P}_\theta &= -\frac{\partial H}{\partial \theta} \\ \dot{\zeta} &= \frac{\partial H}{\partial P_\zeta} \qquad & \dot{P}_\zeta &= -\frac{\partial H}{\partial \zeta}. \end{aligned} \tag{4}$$

Equations for advancing particle positions in time, also in the presence of flute-like perturbations of the form $\delta\vec{B} = \nabla \times \alpha\vec{B}$ with $\vec{B}$ the equilibrium field and $\alpha = \sum_{m,n} \alpha_{m,n}(\psi_p) sin(n\zeta - m\theta - \omega_n t)$ can easily be derived. In addition, for ideal MHD perturbations the rapid mobility of the electrons makes the electric field experienced by the ions parallel to the magnetic field equal to zero. For this representation of $\delta\vec{B}$ it is necessary to add an electric potential Φ to cancel the parallel electric field induced by $d\vec{B}/dt$, with

$$\sum_{m,n} \omega B \alpha_{m,n} e^{i(n\zeta - m\theta - \omega t)} - \vec{B} \cdot \nabla\Phi/B = 0, \tag{5}$$

where we have neglected terms of order α^2. In Boozer coordinates, used in our simulations, taking $\Phi = \sum_{m,n} \Phi_{m,n} e^{i(n\zeta - m\theta - \omega t)}$ the solution is

$$(gq + I)\omega\alpha_{m,n} = (nq - m)\Phi_{m,n}, \tag{6}$$

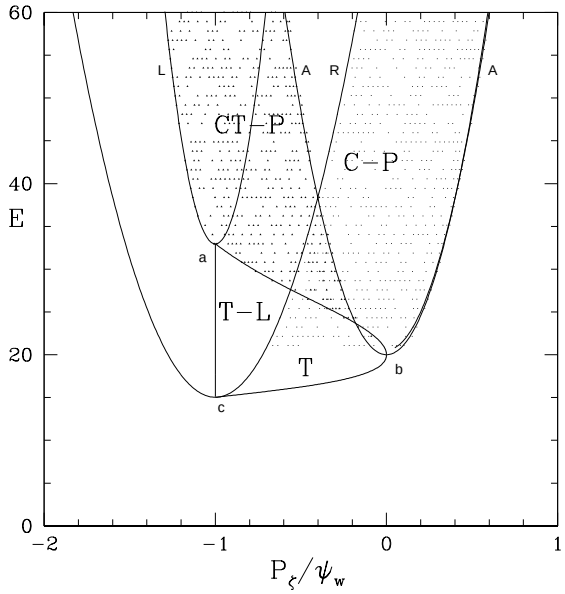

FIG. 1: Plane of P_ζ, E for a range of 20 to 60 keV with $\mu B_0 = 20$ keV, showing domains of confined particles. Shown are co-passing (C-P), counter passing (CT-P), trapped (T) and trapped loss (T-L) domains. The apexes of the parabolas are at $E = \mu B_{max}$ (a), $E = \mu B_0$ (b), $E = \mu B_{min}$ (c).

but in general coordinates where $I = I(\psi, \theta)$ the solution is complicated by the coupling of different poloidal harmonics. The guiding center equations including MHD perturbations are realized using a fourth order Runge-Kutta method in the code ORBIT[5]. The units are conveniently defined by the on-axis gyro frequency (time) and the major radius (distance).

The magnetic moment μ is conserved by the interaction of a particle with a mode with frequency much smaller than the cyclotron frequency, so only P_ζ and E are modified by interaction with it. For a given equilibrium and a fixed value of μ the domains of confined particles in the P_ζ, E plane are given by parabolas defining orbits that make contact with the magnetic axis, the low field side outer boundary, and the high field side outer boundary and the trapped-passing boundary.

An example is shown in Fig. 1 for the DIII-D reversed shear equilibrium in shot 122117 during the period $t = 340 - 370$ $msec$ with $q = 4.7$ on axis and $q = 9$ at the plasma boundary. The plane of P_ζ, E is shown for $\mu B_0 = 20keV$, with B_0 the field strength on axis, and the particle distribution is limited to a maximum energy of 60 keV. The canonical momentum is normalized to the value of flux at the last closed flux surface, ψ_w. The apex of

the parabolas are at $E = \mu B_{max}$ (label a) for the high field side (left edge, label L), $E = \mu B_0$ (label b) for the magnetic axis (label A), and $E = \mu B_{min}$ (label c) for the low field side (right edge, label R). The confined counter passing and co-passing orbits share a common triangular region, in which they have the same values of P_ζ and E but opposite signs of pitch. The full distribution of confined orbits with $\mu B_0 = 20keV$ is shown shaded in Fig. 1. In our simulations we will be using particle distributions produced by NUBEAM[6] in the code TRANSP[7], which calculates the high energy beam distribution produced by neutral beam injection, but does not take account of the presence of MHD modes.

Individual modes produce islands in the phase space of the particle orbits, which through phase mixing produce local flattening of the particle distribution. In addition, overlap of these islands[8, 9] leads to stochastic transport of particles.

We are interested in the case of the interaction of particles of arbitrary pitch with modes of nonzero frequency. It is fairly easy to assess the effect of a particular mode of toroidal mode number n and frequency ω_n on a particle distribution by examining a Poincaré plot for a particular choice of either co-moving or counter-moving particles, which we refer to as a kinetic Poincaré plot to distinguish it from a plot of the magnetic field. Points are plotted in the poloidal cross section whenever $n\zeta - \omega_n t = 2\pi k$ with k integer, where ζ is the toroidal particle coordinate, and ω_n is the mode frequency. Such a plot shows the canonical division of orbits into those following good Kolmogorov Arnold Moser[10] (KAM) surfaces, isolated islands bounded by separatrices, and stochastic domains.

In a previous paper[4] we introduced a general method for numerically determining the existence of or the destruction of good KAM surfaces. Consider following two orbits located very nearby one another in the P_ζ, θ plane, and define the angle χ to give the orientation of the vector joining them in this plane. If good KAM surfaces exist χ can change by at most an angle of π, due to their relative velocity in θ. However two orbits within an island rotate around one another with χ increasing with the rotation about the island O-point, also refered to as the bounce frequency of a particle trapped in the wave, which increases with the size of the island. This is illustrated in Fig. 2, showing vectors between nearby points in the P_ζ, θ plane on good KAM surfaces and in a resonance. The rate of change of χ is a function of distance from the island O-point, dropping to zero at the separatrix. Also, as shown previously[4] χ also rotates without bound in a stochastic domain. Thus we determine the nonexistence of good KAM surfaces by examining nearby pairs of orbits,

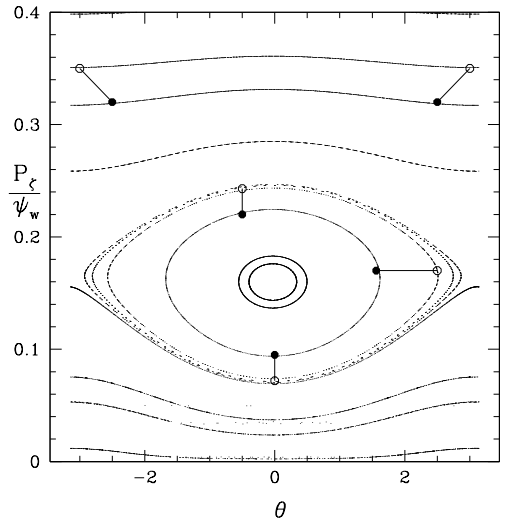

FIG. 2: The P_ζ, θ plane showing a single $n = 1$ resonance island, and vectors between nearby points on good KAM surfaces and in the island. The phase vector between points on nearby KAM surfaces can rotate by at most π, whereas a phase vector in an island rotates through 2π with a period given by the trapping bounce time.

looking for phase vector rotation χ exceeding π. In the present work we take $|\chi| > 4$ to indicate destroyed KAM surfaces. The method of launching closely spaced pairs of orbits spanning the entire space of confined particles was discussed previously[4]. The sensitivity and accuracy of this method for determining domains of non KAM surfaces in the P_ζ, E plane can be ascertained by examining kinetic Poincaré plots in the P_ζ, θ plane along lines given by $\omega P_\zeta - nE = c$.

Of particular importance are cases with a large spectrum of very small amplitude modes, as evidenced by experiments on DIII-D. As an example we choose a case previously discussed in[2, 3], where many modes produced significant modification of the beam distribution. As pointed out previously, this is a difficult trial case, because the mode spectrum is very near stochastic threshold for particle transport, making the results sensitive to small modifications.

III. EQUILIBRIUM, MODES AND PARTICLE DISTRIBUTION

The low shear elliptically shaped equilibrium in DIII-D shot 122117 is shown in Fig. 3, along with the q profile. A reversed shear equilibrium of this sort is particularly unstable

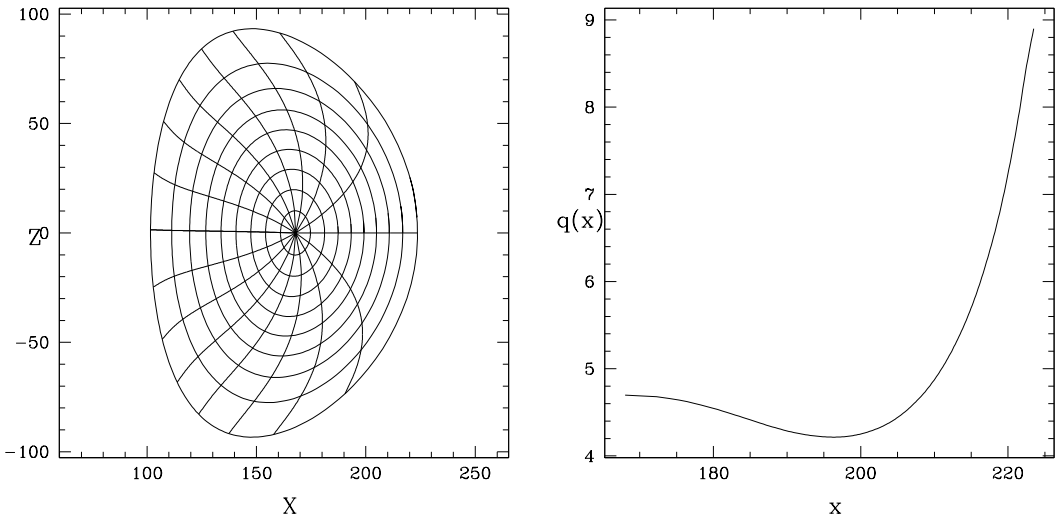

FIG. 3: DIIID equilibrium and q profile

to toroidal Alfvén eigenmodes[11] (TAE) and reversed shear Alfvén eigenmodes (RSAE). The mode spectrum and radial eigenfunctions were obtained with the code NOVA[11], and there has been detailed comparison of these mode structures with experiment using electron cyclotron emission spectroscopy [12–14]. The mode spectrum consisted of eleven TAE and RSAE modes with frequencies ranging from 50 to 100 kHz. Each mode has a fixed toroidal mode number n and a frequency ω, along with approximately 10 poloidal harmonics. An example of the radial profiles of the poloidal harmonics is shown in Fig. 4. Note that this mode is well localized near the plasma center, as were most of the modes in this discharge. An exception was one TAE mode with $n = 6$, $26 \leq m \leq 39$ at 89.4 kHz which was fairly broad radially and was responsible for much of the induced loss.

The beam particle distribution at the time of the observation of the mode spectrum is shown in Fig. 5, generated by TRANSP by the production of a list of 10^6 particles, and using beam deposition physics which ignores the presence of the modes. It is seen that the pitch distribution is strongly peaked, with μB_0 peaked around 20 keV. Maximum beam energy was 80 keV. For the present analysis particle energies are considered only between 20 and 80 keV.

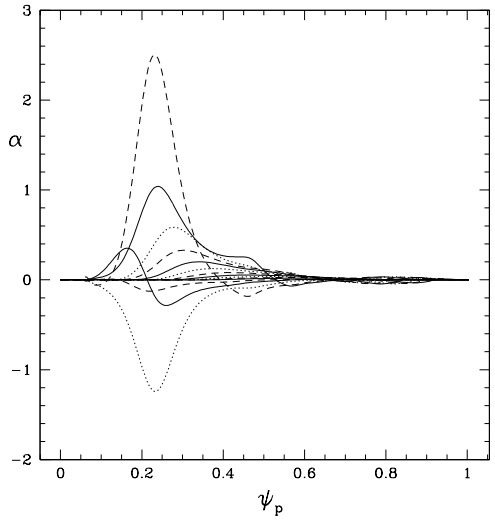

FIG. 4: The poloidal harmonics of an 81 kHz TAE mode, ($\times 10^6$)

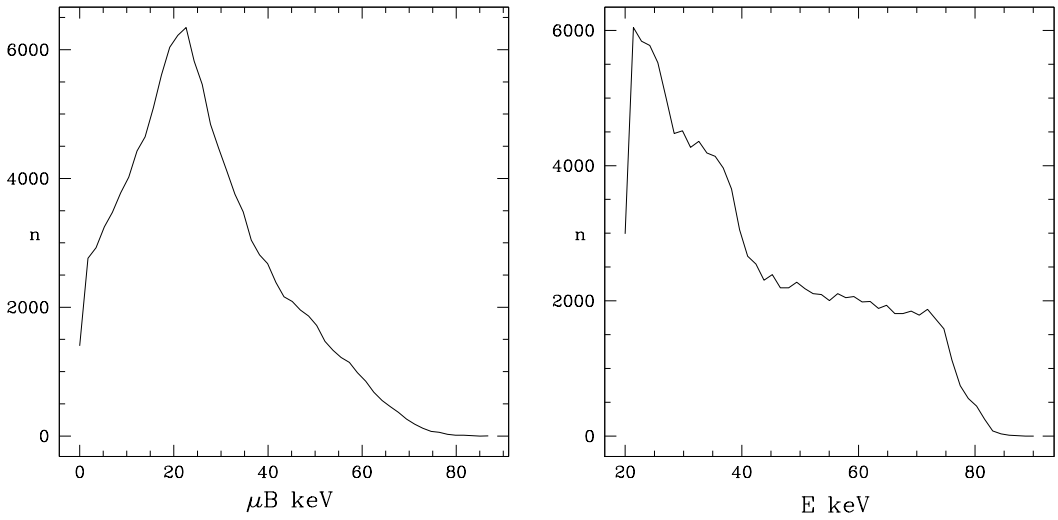

FIG. 5: DIIID beam distributions in μB and E

IV. RESONANCES

We first examine the resonances due to the mode spectrum using both the phase vector rotation and kinetic Poincaré plots, to check the validity of the use of the rotation to determine broken KAM surface domains. It is known that the resonance islands are mostly very small, requiring a fairly long running time to observe phase vector rotation as well as requiring closely alligned pairs of orbits. We divide the distribution in μ into 12 domains, each with a range of 4 keV for μB_0. Since each mode must be examined alone, there are a

total of 132 cases in order to survey the whole distribution.

It is impossible to show the resonant domains of all 11 modes in all 12 domains of μ. To demonstrate the method we select a representative mode, an 81 kHz TAE mode with n = 3, $10 \leq m \leq 23$, the poloidal harmonics of which are shown in Fig. 4, and show the effect of this mode for three different values of μ. Some modes resonate with the distribution much more than others, and also the values of E, P_ζ and μ at which resonances occur varies with frequency, harmonic content, and radial mode structure. The determination of resonance was made using 100 domains in energy and 100 domains in P_ζ and launching pairs of orbits for all confined particles as described previously[4]. We used two orbit pairs for each domain, with different values of ζ, to change the phase of the orbit with respect to the mode, and the pair spacing was $\Delta\psi_p = 2 \times 10^{-4}\psi_w$ with ψ_w the poloidal flux at the last closed flux surface. These parameters as well as the length of time the particles are followed determine the resolution of resonance determination. These plots were made using a time of 400 toroidal transits.

Shown in Fig. 6 is the result of the phase vector rotation determination for a value of μB_0 of 2 keV, and three kinetic Poincaré plots showing the nature of the resonances with energies at the left end of the Poincaré line of 60, 30 and 27 keV. Since we are only interested in particles with energy above 20 KeV there is no trapped domain in this P_ζ, E plot. Although there are many poloidal harmonics in the simulation, there is no observed stochastization of orbits, simply the production of significant islands primarily deep in the plasma interior. The first Poincaré figure, showing the plot for the line starting at 60 keV, shows 13 small islands at P_ζ = -0.02, 12 at P_ζ = 0.085, and 11 at 0.24, these resonances being also visible in the P_ζ, E plane. There are some breaks in the resonance lines in the P_ζ, E plane due to insufficent resolution, which could be improved by a greater density of orbit pairs. The second plot, for the Poincaré line starting at 30 keV, shows 12 small islands at P_ζ = -0.19, 11 at -.04, and two large 10 island structures at 0.28 and 0.4. The last plot, for the line starting at 20 keV, shows 10 small islands at P_ζ = 0.09, and 10 islands at P_ζ = 0.4 . The large resonance near the magnetic axis in the P_ζ, E plane is a 10 island structure for all energies, but bifurcates at $E = 40keV$ into two distinct resonances for lower energy.

Shown in Fig. 7 is the result of the phase vector rotation determination for a distribution with μB_0 of 22 keV, and three kinetic Poincaré plots showing the nature of the resonances with energies at the left end of the line of 60, 30 and 23 keV. The first figure, showing the

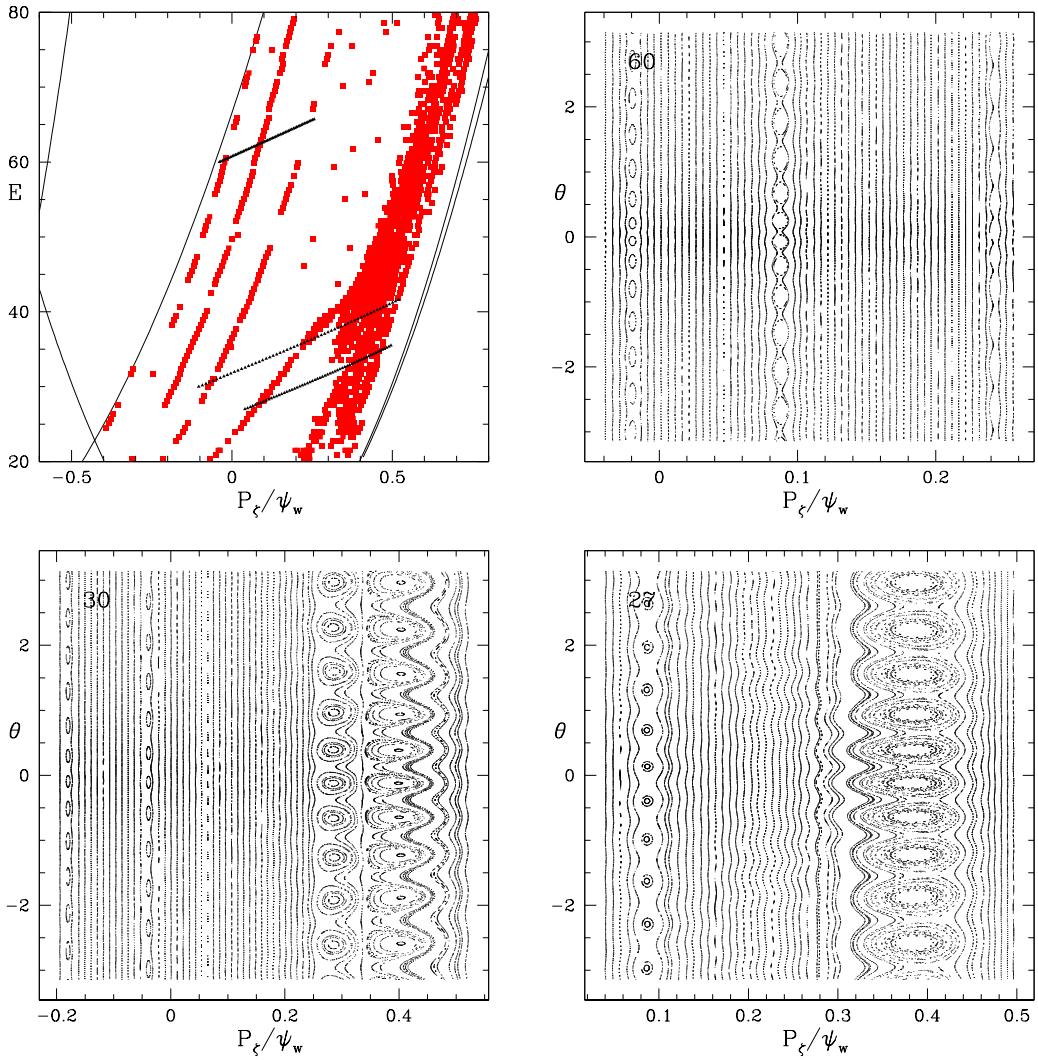

FIG. 6: Plane of P_ζ, E with $\mu B_0 = 2KeV$, for an 81 kHz TAE mode with n = 3, $10 \leq m \leq 23$, showing paths for kinetic Poincaré plots for the three lines, originating at the left end at 60, 30 and 27 keV.

Poincaré plot for the line starting at 60 keV, shows a large island at $P_\zeta = 0.52$ and smaller islands at -0.01, 0.04 and 0.34. The second plot, for the Poincaré line starting at 30 keV, shows an 8 island chain at $P_\zeta = 0.08$, a 9 island chain at $P_\zeta = 0.28$, and the first order 17 island Fibonacci chain produced by these at $P_\zeta = 0.18$. The last plot, for the line starting at 23 keV, shows 3 large islands at $P_\zeta = -0.57$, 4 islands at $P_\zeta = -0.48$, and also many smaller islands for higher values of P_ζ. These smaller resonance islands are not individually resolved in the P_ζ, E plane.

In Fig. 8 are results of KAM destruction and associated Poincaré plots for $\mu B_0 = 46KeV$,

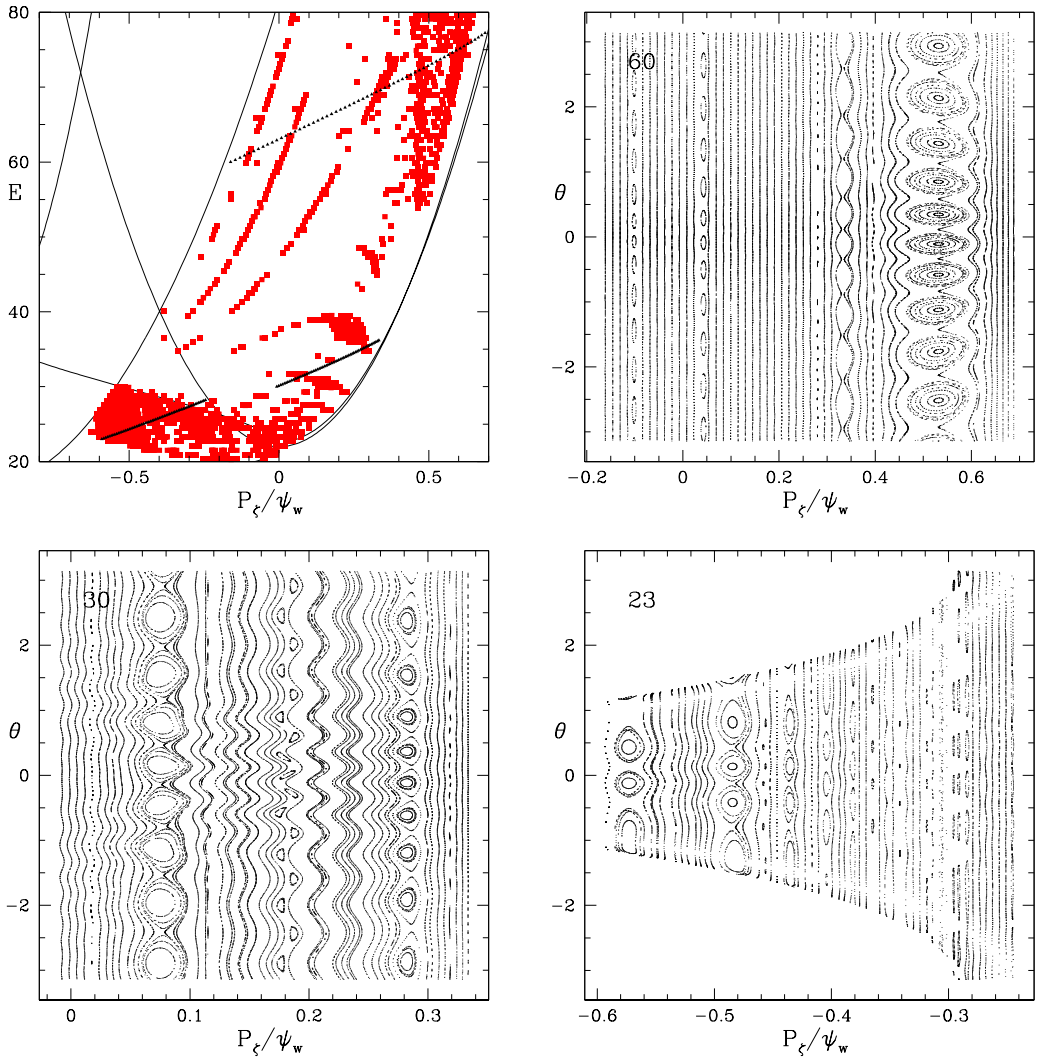

FIG. 7: Plane of P_ζ, E with $\mu B_0 = 22KeV$, for an 81 kHz TAE mode with $n = 3$, $10 \leq m \leq 23$, showing paths for kinetic Poincaré plots for three lines originating at the left end at 60, 30 and 23 keV

showing significant mode-particle interaction near the trapped-passing boundary, perhaps because the large variation of the parallel velocity over the orbit allows the possibility of resonance at some point. In the first Poincaré plot, starting at 59 keV, there is a large 9 island chain at $P_\zeta = 0.33$, and a smaller 8 island chain at $P_\zeta = -0.02$. In the second Poincaré plot, starting at 50 keV, there are trapped particle resonances at $P_\zeta = -0.46$ and $P_\zeta = -0.4$, and many closely spaced resonances just above this. These smaller resonance islands are not individually resolved in the P_ζ, E plane. In the third Poincaré plot, starting at 43 keV, there is a trapped particle resonances at $P_\zeta = -0.2$ and a fully stochastic domain

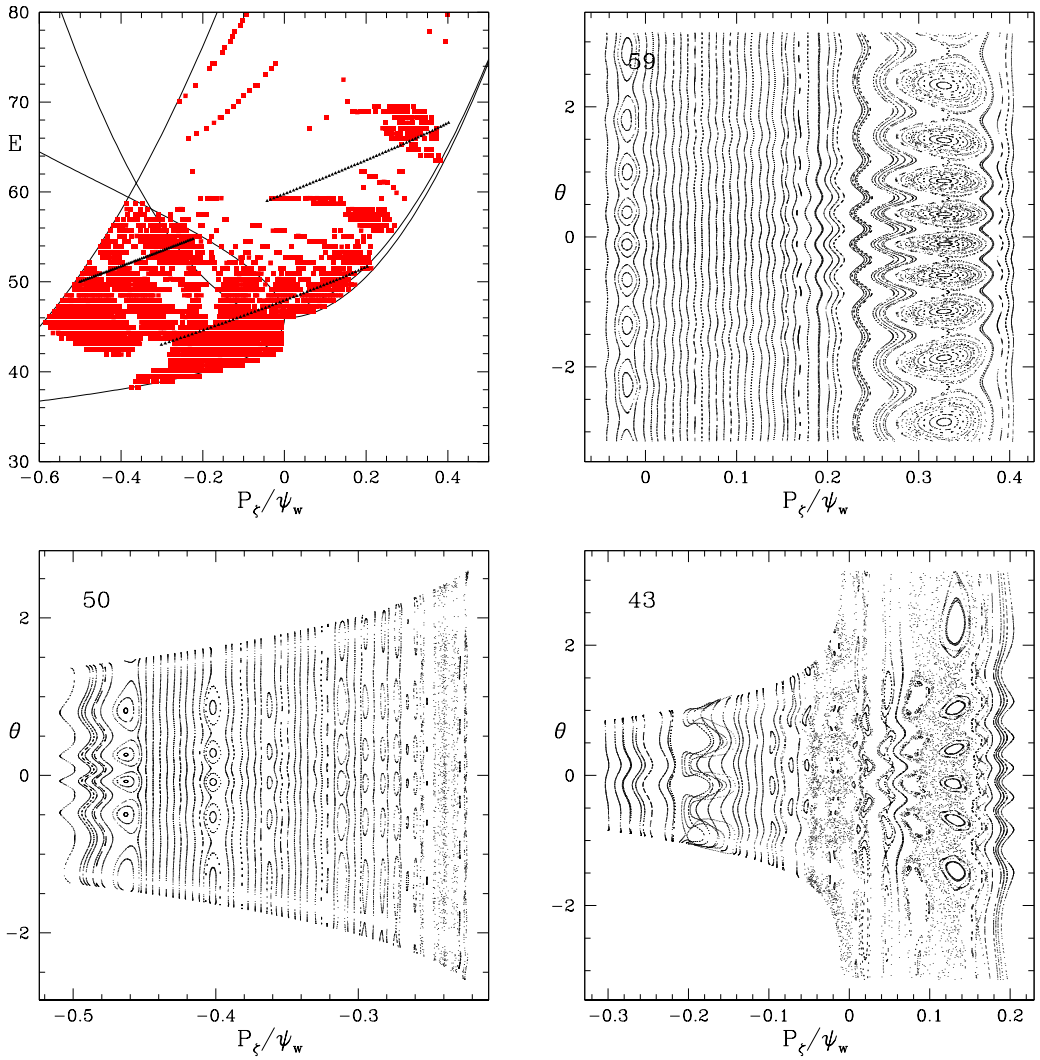

FIG. 8: Plane of P_ζ, E for $\mu B_0 = 46KeV$, with an 81 kHz TAE mode with n = 3, $10 \leq m \leq 23$, showing paths for kinetic Poincaré plots for three lines, originating at the left end at 59, 50 and 43 keV, and the kinetic Poincaré plot for these lines

with some remnant island structures just inside the passing particle domain.

These kinetic Poincaré plots demonstrate that the phase vector rotation gives an accurate determination of the location and size of islands and stochastic domains, limited only by the resolution chosen for the evaluation. It is interesting that in this case the distribution modification is achieved by these modes through a large density of non overlapping island structures, without extensive stochastic regions produced by each mode alone. As shown in[4], different modes which have island structures at the same values of P_ζ, E produce stochastic transport agreeing with quasilinear estimates in the limited domain spanned by

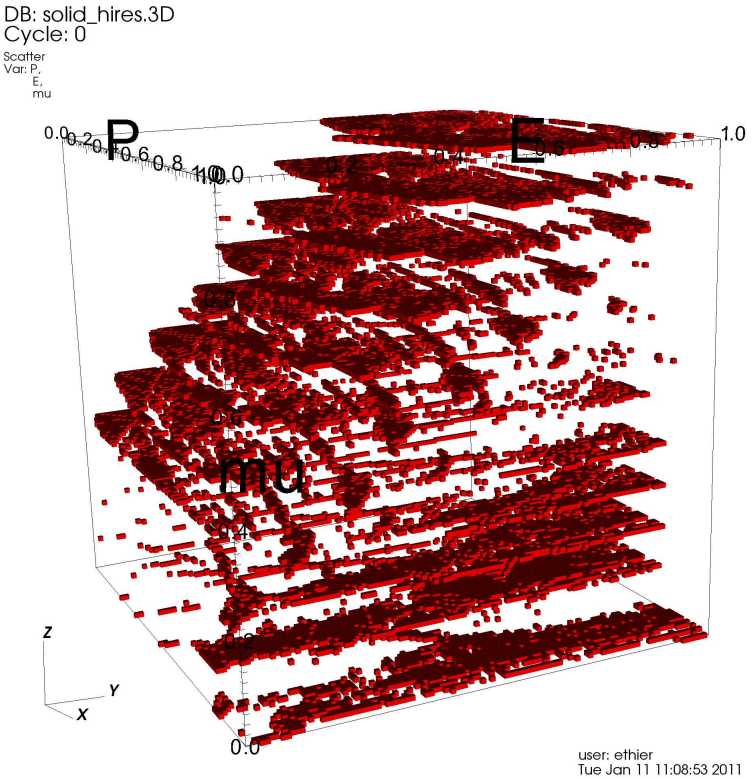

FIG. 9: An example of the full resonance domain of an 81 kHz TAE mode on the particle distribution. Space is left between the different values of μ, to allow visualization. Actually the resonant structures are fused in μ to form connected localized blocks.

the island structures.

In Fig. 9 is a full 3D plot of this mode in the space of P_ζ, E, μ, showing the density of resonances produced. Space has been left between the different values of μ, otherwise it is very difficult to envision the space of resonances because it is so dense. The magnetic moment μB_0 is plotted vertically, energy is increasing to the right, and canonical momentum is increasing coming out of the page. The resonances are seen to comprise continuous volumes in the space of P_ζ, E, μ. As μ increases they move to larger energy, being associated with a particular value of $v_\parallel$.

V. TIME ANALYSIS FOR PHASE VECTOR ROTATION

The only computationally demanding part of the analysis in this work is the determination of the domains of non KAM surfaces. Thus it is important to find the number of toroidal

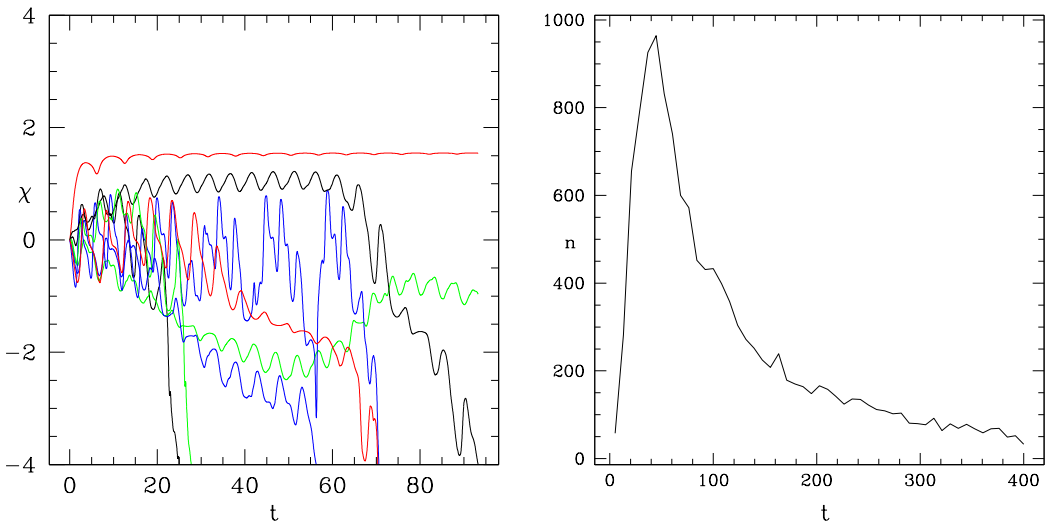

FIG. 10: Time history of $\chi(t)$ for some orbit pairs, plotted versus toroidal transits, showing some trajectories reaching $|\chi| = 4$, and the distribution of times for orbit pairs to reach $|\chi| = 4$, plotted versus toroidal transits, particles taking approximately one microsecond per transit.

transits necessary to follow orbit pairs in order to discover all important resonances. In Fig. 10 is an example of the time histories of χ for five different orbit pairs, three of which reach the critical limit of $|\chi| = 4$. Once a trajectory has become resonant χ very rapidly exceeds this value, as seen by the almost vertical behavior of the plots approaching the limiting value. Also shown is the distribution of times for orbit pairs to reach $|\chi| = 4$, plotted versus toroidal transits, particles taking approximately one microsecond per transit. For the resolution used all domains of destroyed surfaces are found by 400 transits, or about 0.4 msec. It is misleading to think simply of a progression of orbit pairs as shown in Fig. 2, because the two particles do not remain in phase in toroidal angle ζ, and thus do not appear simultaneously in any given Poincaré section. Thus the angle χ does not rotate uniformly in time for an orbit pair in an island, the time history of the rotation is more complicated, and in fact it is somewhat mysterious the accuracy with which the vector rotation indicates the location of resonances.

An analysis of the time evolution of the orbit differentials ΔP_ζ, $\Delta\zeta$, $\Delta\theta$, $\Delta\psi_p$ has been started, to see whether any simplification or insight into the dynamics of the phase vector rotation can be obtained. It has been verified that all these quantities remain small during the whole orbit pair evolution, so that a differential analysis is appropriate.

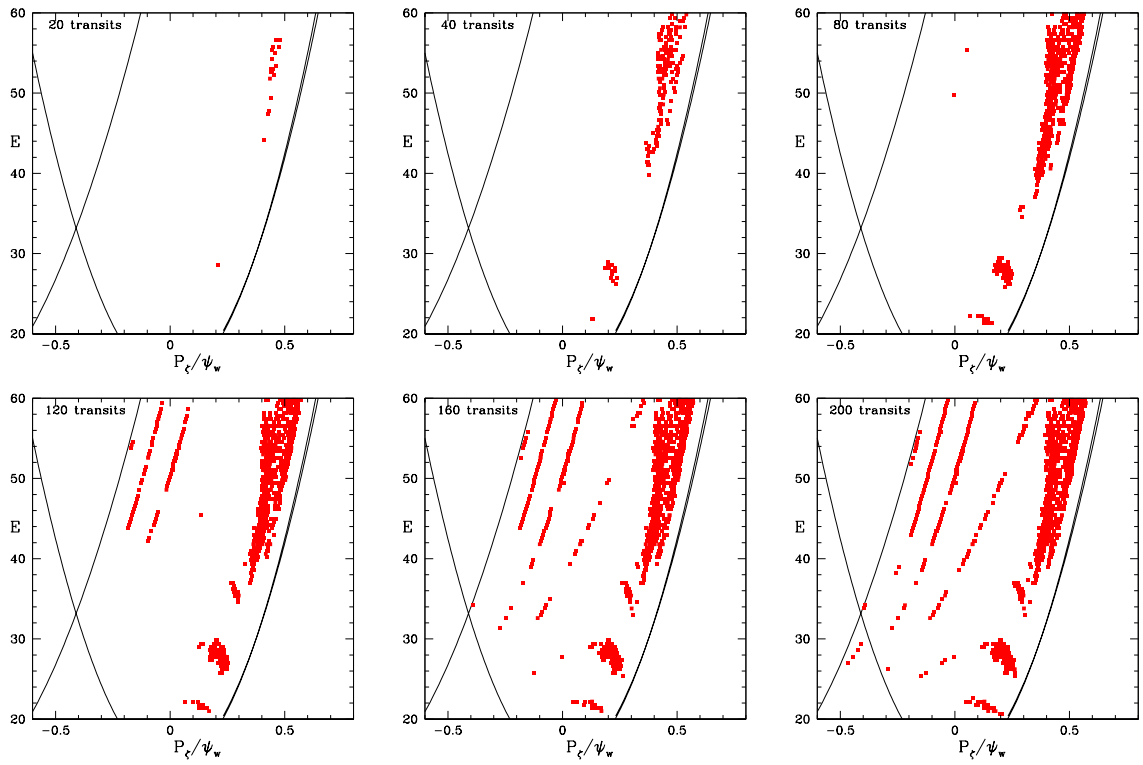

FIG. 11: Plane of P_ζ, E for $\mu B_0 = 14keV$ at different times, showing the rapid filling in of the large islands, followed later by the smaller ones. The mode is an 81 kHz TAE mode with $n = 3$ and $10 \leq m \leq 23$. One transit equals approximately one microsecond.

In Fig. 11 are shown the points in the P_ζ, E plane at which orbit pairs have reached $|\chi| = 4$ for different times. The centers of large islands, with the most rapid phase vector rotation, are the first to appear. At later times the parts of large islands closer to the separatrix appear, as well as smaller islands.

There is a limit on the time of search for phase vector rotation imposed by the resolution of the grid used in the P_ζ, E plane. In Fig. 12 is an island chain that is detected with phase vector rotation only after 80 toroidal transits. It has a width of $P_\zeta = .01\psi_w$. When such an island is detected it causes the whole domain in the P_ζ, E plane to be labelled stochastic. Thus it should not be counted if the domain size in P_ζ is larger than $.01\psi_w$, otherwise such islands give an overestimation of the degree of stochastization caused by the modes. We take the criterion that the islands detected must be more than half the size of the domain in the P_ζ, E plane to cause that domain to be labelled stochastic. Also shown are two examples of dense but nonoverlapping island chains, one in the passing domain and one in

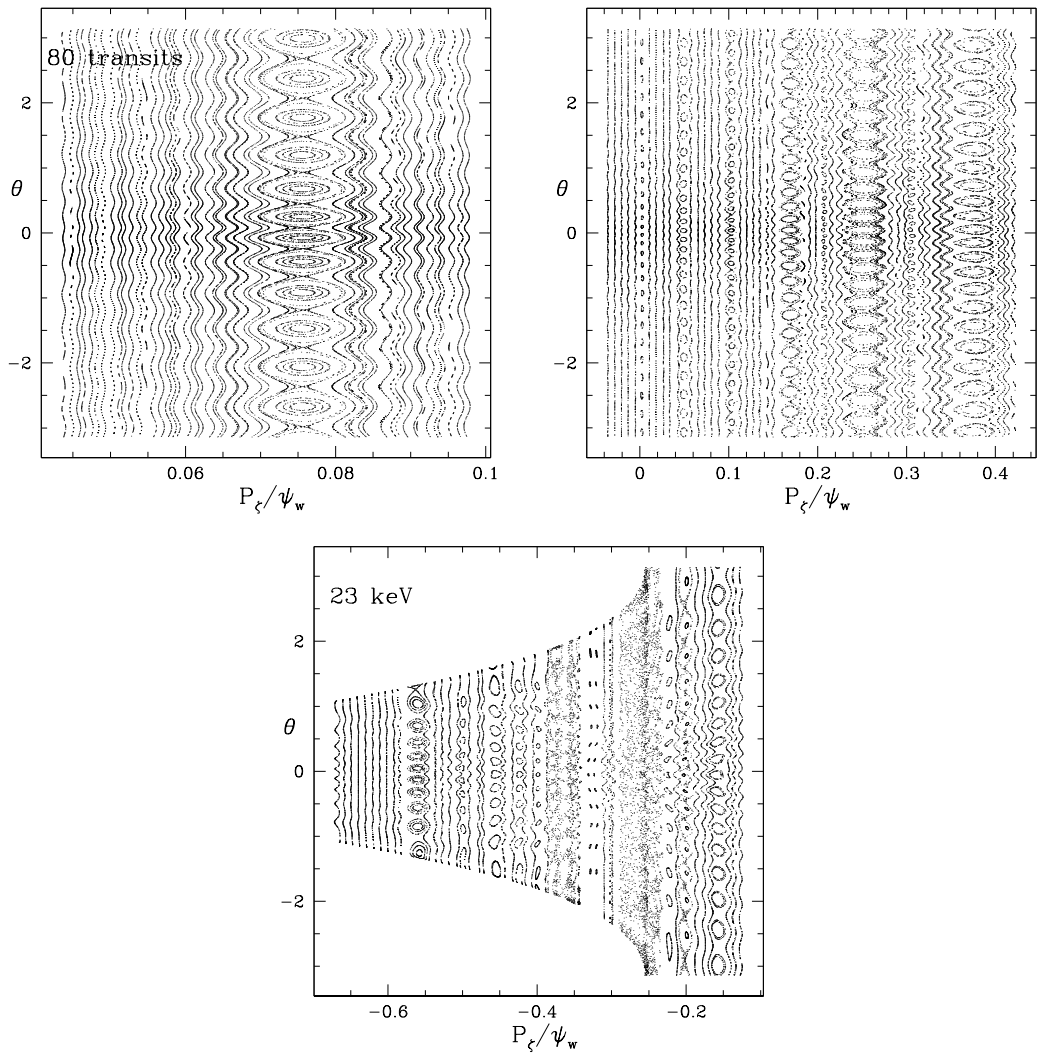

FIG. 12: An island chain that first appears with phase vector rotation after 80 transit times with width of $P_\zeta = .01\psi_w$, and examples of dense but nonoverlapping island chains, the first due to an 89.4 kHz mode with $n = 6$ and $26 \leq m \leq 39$, and $22 \leq m' \leq 27$, showing also the first order Fibonacci chains of $m'/n = 45/12$ and $m'/n = 47/12$. The third example shows closely spaced resonances in the trapped particle domain, which would indicate a completely stochastic region if the domain spacing in ΔP_ζ were greater than $0.01\psi_w$.

the trapped domain. A resolution in the domains with $\Delta P_\zeta > .01\psi_w$ would indicate that the whole domain was stochastic and produce an overestimation of the transport. A knowledge of the details of the mode spectrum can save greatly on the computing time necessary to find the ability of the modes to modify the particle distribution and is necessary in order to avoid overestimation of transport. If the P_ζ, E plane shows a domain to be completely

stochastic it must be investigated using a kinetic Poincaré plot to be certain that in fact the island chains do overlap. Very small islands which do not overlap can be eliminated from the annealing process by restricting the time allowed for $|\chi| = 4$ to be achieved, as shown in Fig. 11. The data set listing the orbit pairs for which $|\chi| > 4$ contains the mode number, the initial P_ζ, E, μ coordinates, and the time, so such a limitation can be imposed without a repetition of the numerical simulation.

VI. ANNEALING AND LOSS

We wish to use the determination of domains in the P_ζ, E plane with destroyed KAM surfaces to find the evolution in time of an initial distribution under the action of a given mode spectrum as well as the distribution of lost particles if the resonances cause loss. We are interested in collisionless effects, but we point out that pitch angle scattering, since it conserves energy, results in simple diffusion in P_ζ and μ, and can be included. Similarly it is simple to include the effect of energy loss through slowing down on electrons. A final state exists only if the phase space does not allow continuous loss. Otherwise time must be taken into account and relevant diffusion rates used to find the distribution at a given time.

Construct a numerical method of producing the evolution of an initial particle distribution under the action of a given spectrum of modes. The function of a particular mode with frequency ω and toroidal mode number n is to equilibrate particle density in all adjacent island and stochastic domains along lines given by $\omega P_\zeta - nE = constant$, since this combination is conserved and annealing can happen only along this line. However, as shown in[4] repeated annealing for multiple modes, with different values of ω/n, produces diffusive motion in the combined non-KAM domains of the modes involved, at the level given by a quasilinear approximation. Thus the necessary algorithm must be an iterative annealing process, one mode at a time, but repeated so as to capture the diffusion produced by the combination of modes present.

Examine a high energy particle distribution as predicted by a neutral beam deposition calculation or an alpha particle birth profile calculation, and make a number of domains in the magnetic moment μ sufficient to give a good representation of the distribution. For each μ, divide the space of confined particles in the P_ζ, E plane into small domains, with size determined by the desired resolution of small islands. Then find the domains of broken KAM

surfaces for that part of the plane which is occupied by the distribution by following pairs of orbits and looking for phase vector rotation, noting whether each domain is stochastic or consists of good KAM surfaces. This is the only computationally demanding part of the calculation, depending on the desired resolution for island size. The island size resolution, and thus the number of toroidal transits that the orbit pairs should be followed, is determined by the size of the P_ζ, E domains. Islands much smaller than the domain size should not be counted, as noted in the discussion concerning Fig. 12.

Reintroduce the original particle distribution and partition it into the μ, P_ζ, E domains. At this point, to improve accuracy of the annealing process the number of particles can be multiplied by a factor sufficient to make the number of particles in each domain large. Then carry out an equilibration of densities in stochastic domains which are in contact along lines $\omega P_\zeta - nE = c$ for each mode. Each iteration of this process corresponds to a diffusion step of ΔP_ζ, the size of the domains in the P_ζ, E plane.

To carry out the equilibration, note that the differential volume is given by $dV \sim J(\psi_p, \theta) d\theta d\psi_p$, where in Boozer coordinates $JB^2 = gq + I$. Thus the domain at μ, P_ζ, E with range dP_ζ has volume

$$dV \sim dP_\zeta \int d\theta \left(\frac{d\psi_p}{dP_\zeta}\right)_{E,\mu} J(\psi_p, \theta), \tag{7}$$

the integration being over the particle orbit. Using $P_\zeta = g\rho_\parallel - \psi_p$ and $E = \rho_\parallel B^2/2 + \mu B$ we find

$$dV = dP_\zeta \int d\theta \frac{(gq + I)}{B^2} \frac{1}{1 + g(\rho_\parallel^2 B + \mu)\partial_{\psi_p} B/\rho_\parallel B^2 - g'\rho_\parallel} \tag{8}$$

where the integral is taken over a constant μ, P_ζ, E surface, *ie* along the particle orbit, and $g' = \partial_{\psi_p} g$. Consider neighboring stochastic domains along the lines with $\omega P_\zeta - nE = c$ with initial particle numbers in the domains n_1, n_2 and $n_1 + n_2 = N$. The new particle numbers n_1', n_2' by particle conservation satisfy $n_1' + n_2' = N$ and setting densities equal gives $n_1'/dV_1 = n_2'/dV_2$ so the new particle numbers are

$$n_1' = \frac{N dV_1}{dV_1 + dV_2}, \qquad n_2' = \frac{N dV_2}{dV_1 + dV_2}. \tag{9}$$

In addition to replacing the particle numbers in adjacent stochastic domains with the modified values for the two domains, stochastic domains in contact with the last closed flux surface are emptied of particles, they being counted as lost. This process must be repeated

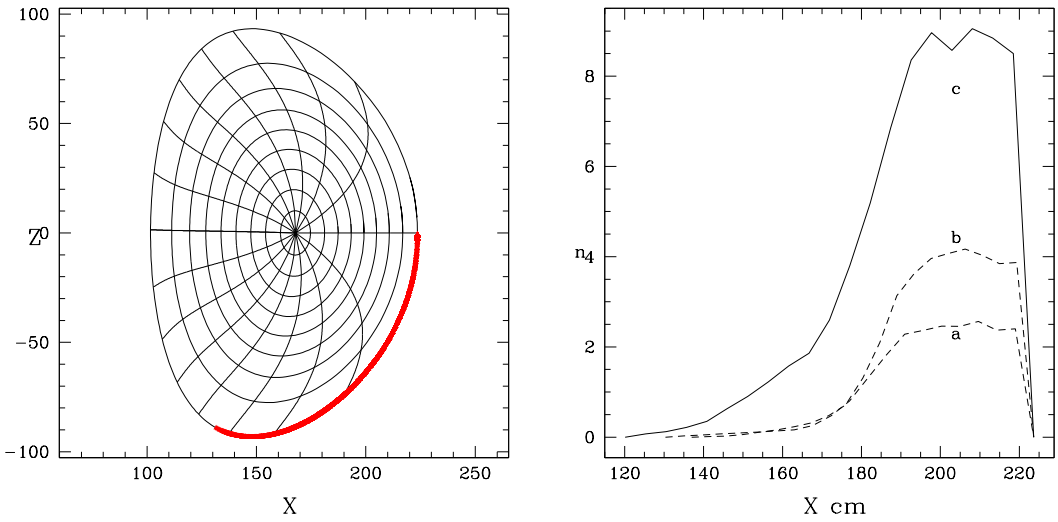

FIG. 13: The locations of lost particles on the last flux surface, and the distribution of lost particles with respect to major radius X, with dB/B equal to (a) 2×10^{-4}, (b) 3×10^{-4}, and (c) 4×10^{-4}.

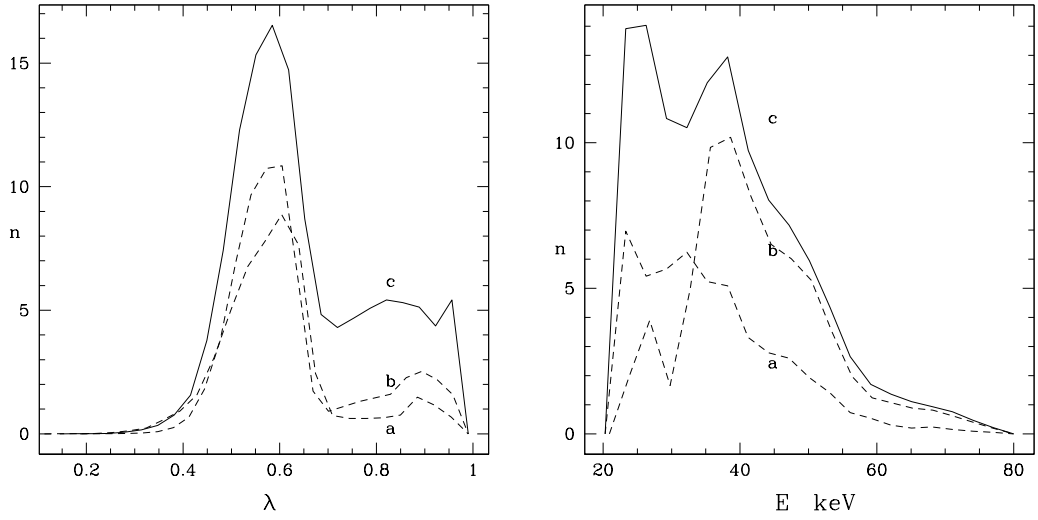

FIG. 14: The distributions of lost particles in pitch λ and in energy E, with dB/B equal to (a) 2×10^{-4}, (b) 3×10^{-4}, and (c) 4×10^{-4}.

many times using the stochastic domain template for each mode. Each step of the annealing process corresponds to a diffusion step size of one domain ΔP_ζ. The time corresponding to diffusion through ΔP_ζ is given by the quasilinear rate for the mode[4], also roughly of the same order as the Landau relaxation time for phase mixing in an island.

After any number of annealing steps the remaining confined particle distribution can

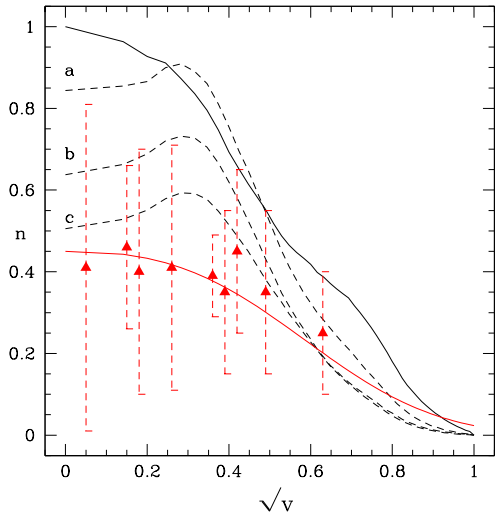

FIG. 15: The initial DIII-D particle distribution and final distributions after 600 annealing steps, in this case corresponding to about 60 msec, with dB/B equal to (a) 2×10^{-4}, (b) 3×10^{-4}, and (c) 4×10^{-4}. Also shown, with rather large error bars, are the experimental values.

be reconstructed. Given μ, P_ζ, E the orbit is completely determined, but not the particle location on the orbit. Note that these values do not determine the radial profile. For example all particles could be placed at $\theta = 0$, or at $\theta = \pi$, resulting in very different radial profiles. The distribution can be reconstructed using a uniform distribution in θ, giving a reasonable radial profile. Since n_1', n_2' from Eq. 9 are not integer, reconstructing the distribution involves rounding to the nearest integer, hence the reason for making n_1, n_2 large.

It is clearly possible to make the temporal evolution more exact, by using complete equilibration of neighboring stochastic domains only in domains where the quasilinear diffusion is largest. These regions would set the time scale for a single annealing step. Other domains, where the value of the quasilinear diffusion was lower, could be subjected to partial annealing corresponding to the lower diffusion rate. In the present work we simply associate a time scale of 0.1 msec, given by the quasilinear value for diffusion due to the modes for each annealing step.

In a previous work we examined the modification of a particle distribution due to an avalanche produced by a number of overlapping resonances. In this work we focus on the DIII-D case discussed in[2, 3], which provides a difficult test for the method, since the observed spectrum of modes is very near stochastic threshold for distribution modification.

Co-moving passing particles lost at each step of the annealing process pass through the left side of the boundary for confined particles with specific values of P_ζ, E, μ. Orbits at the loss boundary impact the last closed flux surface at the outboard midplane. By assuming particles to continue diffusion in P_ζ after entering on a lost orbit, a distribution in pitch values and impact points is obtained. The time to diffuse through one domain in P_ζ is given by the quasilinear rate, and in this case is approximately one tenth of a millisecond. Thus each iteration of the annealing processs corresponds to a diffusion time step of this magnitude. The flight time once a particle is on a lost orbit is approximately a microsecond. Thus by assigning a random further decrease in P_ζ during the time on the lost orbit, using the ratio of these times, distributions in the energy, pitch, and location are determined. The distributions are shown in Figs. 13 and 14 for simulations of 600 annealing steps, in this case corresponding to about 60 msec with perturbation amplitudes dB/B equal to (a) 2×10^{-4}, (b) 3×10^{-4}, and (c) 4×10^{-4}. Shown is the location of lost particles on the last flux surface, the distribution in major radius, as well as pitch and energy distributions.

Note that if a representation of the magnetic field beyond the last closed flux surface is available, the values of energy, pitch, and location can be used to continue these orbits into the vacuum region to improve strike point information[15].

In Fig. 15 is shown the initial radial distribution and that after 600 annealing steps, in this case corresponding to about 60 msec with perturbation amplitudes dB/B equal to (a) 2×10^{-4}, (b) 3×10^{-4}, and (c) 4×10^{-4} obtained through the annealing process as well as the experimental values. The variable V is the normalized volume contained inside a given flux surface, and is used to label the flux surfaces. The histograms of the particle distribution are made using bins of equal size in V, and the result plotted vs $\sqrt{V}$, approximately equal to the minor radius. It is clear from these figures that there is a stochastic threshold for significant loss at about $dB/B = 2 \times 10^{-4}$, with collisionless transport increasing rapidly for TAE amplitudes above this. Note that this is a difficult test case because the modes are very near stochastic threshold for particle transport, making the results sensitive to small changes. The inclusion of pitch angle scattering, not present in these simulations, would further smooth and lower the profiles.

VII. CONCLUSION

In conclusion, we have extended the method for the determination of domains of broken KAM surfaces in the space of P_ζ, E, μ describing confined particles in a toroidal confinement device due to the presence of a spectrum of MHD modes given in [4]. We have described the application of the method to a previously studied and well documented case of toroidal Alfvén modes in the DIII-D tokamak[2, 3]. This method gives a clear detailed understanding of the effect of each mode on the particle distribution, and shows which modes produce losses as well as what part of the distribution is lost. It also reasonably reproduces the main results of a full guiding center simulation, and gives the possibility of rapid evaluation of particle loss. The main computing requirement is the following of the orbit pairs to produce the non-KAM domains. For the annealing shown in Fig. 15 20,000 particle pairs were followed for 100 toroidal transits, or about 0.1 msec, and the computing requirements for the annealing process itself were insignificant, taking only minutes of computing time. On the other hand, the guiding center simulations reported previously[2, 3] followed 10,000 particles for 60 msec. The present method requires orders of magnitude less computing than a full guiding center simulation.

The present method must be understood to give the initial response of a distribution to a spectrum of modes, not a long time simulation of the coupled system. It must be recognized that after significant modification of the distribution the mode spectrum will change, so it does not make sense to continue this process once the distribution is modified. However it gives a means of quickly examining a given particle distribution and mode spectrum to understand whether profile modification would occur. In addition, it is not difficult to imagine for the future an iteration involving the calculation of instabilities produced by a given equilibrium, the evolution of the distribution due to the modes using this method, and a return to calculation of the modified instability spectrum.

Acknowledgement

This work was partially supported by the U.S. Department of Energy Grant DE-AC02-09CH11466.

---

[1] W. W. Heidbrink, *Phys. Plasmas* **15**, 055501 (2008), and references therein.

[2] R. B. White, N. N. Gorelenkov, W. W. Heidbrink, M. A. Van Zeeland, *Phys. of Plasmas* **17** 056107 (2010)

[3] R. B. White, N. N. Gorelenkov, W. W. Heidbrink, M. A. Van Zeeland, *Plasmas Physics Controlled Fusion* **52** 045012 (2010)

[4] R. B. White, *Comm. in Nonlinear Science and Numerical Simulations* **XX** XX (2011)

[5] R. B. White, M.S. Chance, *Phys. Fluids* **27**, 2455 (1984).

[6] Alexei Pankin, Douglas McCune, Robert Andre, Glenn Bateman, and Arnold Kritz, *Comp. Phys. Comm.* **159**, 157 (2004).

[7] R. V. Budny, M. G. Bell A. C. Janos *et al*, *Nucl Fusion* **35**, 1497 (1995).

[8] M. N. Rosenbluth, R.Z Sagdeev, J.B. Taylor, G M Zaslavsky *Nuclear Fusion* **6** 297 (1966)

[9] B. V. Chirikov, *Phys. Rep.* **52** 263 (1979)

[10] A. N. Kolmogorov, *Proc. Int. Congr. Mathematicians, Amsterdam, Vol 1* 315 (1957), V. I. Arnold, *Russ. Math. Surv.* 18(5):9, 1963, J. Moser, *Math. Phys. Kl. II 1,1 Kl(1):1*, 1962.

[11] C. Z. Cheng, *Phys. Rep.* **211** 1-51 (1992)

[12] M. A. Van Zeeland, et al, *Phys. Rev Lett.* **97**, 135001 (2006).

[13] M. A. Van Zeeland, et al., *Phys. Plasmas* **14**, 056102 (2007).

[14] M. A. Van Zeeland, W.W. Heidbrink, R. Nazikian, et al, *Nucl. Fusion* **49**, 065003 (2009).

[15] D. C. Pace et al, *IAEA Conference Daejeon* **2EXW/4-2** (2010)

The Princeton Plasma Physics Laboratory is operated
by Princeton University under contract
with the U.S. Department of Energy.

Information Services
Princeton Plasma Physics Laboratory
P.O. Box 451
Princeton, NJ 08543

Phone: 609-243-2245
Fax: 609-243-2751
e-mail: pppl_info@pppl.gov
Internet Address: http://www.pppl.gov